



**HAL**  
open science

## Photodegradation of Molecular Iodine on SiO<sub>2</sub> Particles: Influence of Temperature and Relative Humidity

A. Figueiredo, Rafal Strekowski, L. Bosland, A. Durand, H. Wortham

### ► To cite this version:

A. Figueiredo, Rafal Strekowski, L. Bosland, A. Durand, H. Wortham. Photodegradation of Molecular Iodine on SiO<sub>2</sub> Particles: Influence of Temperature and Relative Humidity. *Journal of Nuclear Engineering and Radiation Science*, 2021, 7 (3), 10.1115/1.4048846 . hal-03214498

**HAL Id: hal-03214498**

**<https://hal.science/hal-03214498>**

Submitted on 1 May 2021

**HAL** is a multi-disciplinary open access archive for the deposit and dissemination of scientific research documents, whether they are published or not. The documents may come from teaching and research institutions in France or abroad, or from public or private research centers.

L'archive ouverte pluridisciplinaire **HAL**, est destinée au dépôt et à la diffusion de documents scientifiques de niveau recherche, publiés ou non, émanant des établissements d'enseignement et de recherche français ou étrangers, des laboratoires publics ou privés.



Distributed under a Creative Commons Attribution 4.0 International License

1 Photodegradation of molecular iodine on SiO<sub>2</sub> particles: Influence of  
2 temperature and relative humidity  
3

4 A. Figueiredo <sup>a,b</sup>, R.S. Strekowski <sup>\*,a</sup>, L. Bosland <sup>b</sup>, A. Durand <sup>a</sup>, H. Wortham <sup>a</sup>

5 <sup>a</sup> Aix Marseille Univ, CNRS, LCE, Marseille, France

6 <sup>b</sup> Institut de Radioprotection et de Sûreté Nucléaire, PSN-RES/SAG/LETR, Cadarache,  
7 France  
8

9 **Abstract**

10 A molecular derivatization method followed by gas chromatographic separation coupled with  
11 mass spectrometric detection was used to study photo-degradation of molecular I<sub>2</sub> adsorbed on  
12 solid SiO<sub>2</sub> particles. The heterogeneous photo-degradation of I<sub>2</sub> was studied as a function of  
13 temperature and relative humidity in synthetic air to better understand its environmental fate.  
14 Two sets of experiments were carried out. In the first set of experiments, the temperature was  
15  $T = (298 \pm 1) \text{K}$  and relative humidity was varied from  $\leq 2\%$  to 75% RH under given experimental  
16 conditions. In the second set of experiments, the relative humidity within the Pyrex bulb was  
17 40% RH and the temperature was varied from  $283 \pm 1 \leq T(\text{K}) \leq 323 \pm 1$ . The obtained results show  
18 a considerably enhanced atmospheric lifetime of molecular iodine adsorbed on solid media that  
19 does not depend on relative humidity of the environment. The obtained results show that the  
20 rate constant for the photolysis of molecular iodine adsorbed on model SiO<sub>2</sub> particles depends  
21 on temperature and is reported to be  $J(T) = (1.24 \pm 1.4) \times 10^{-2} \times \exp[(1482 \pm 345)/T]/\text{s}$   
22 over the measured temperature range. The heterogeneous atmospheric residence time ( $\tau$ ) of I<sub>2</sub>  
23 adsorbed on solid media is calculated to range from 2 to 4.1 hours. The experimentally obtained  
24 heterogeneous lifetime of I<sub>2</sub> is shown to be considerably longer than its destruction by its  
25 principal atmospheric sink, photolysis. The observed enhanced atmospheric lifetime of I<sub>2</sub> on  
26 heterogeneous media will likely have direct consequences on the atmospheric transport of I<sub>2</sub>  
27 that influences the toxicity or the oxidative capacity of the atmosphere.

## 28 **Introduction**

29 Atmospheric aerosols are known to play important direct and indirect roles in climate regulation  
30 [1]. Aerosols' direct climate regulation properties are attributed to their light-scattering  
31 characteristics and aerosols' indirect effects include their ability to act as cloud condensation  
32 nuclei (CCN), thus, affecting the Earth's energy budget. In turn, aerosols' optical and CCN  
33 properties are governed by their chemical composition and reactivity. Molecular iodine and  
34 other iodine containing organic compounds are known to make up an important fraction of the  
35 marine and coastal sites aerosol content [2]. Ocean emissions account for the majority of  
36 molecular iodine emissions into the natural atmosphere [3,4] with the measured I<sub>2</sub> mixing ratios  
37 ranging from few pptv to 300±100 pptv [5–13]. More recently, molecular iodine emissions have  
38 gained an increased level of interest in the scientific community and executive branches of some  
39 governments following the major nuclear power plant accident in Fukushima (Japan) [14,15]  
40 where significant radioactive molecular iodine and other organic iodides emissions were  
41 observed (among other radioisotope emissions) in the atmosphere when the reactor containment  
42 structure was damaged.

43 While the atmospheric reactivity of gas phase I<sub>2</sub> is now well understood and characterized  
44 [12,16], our understanding of the heterogeneous reactivity on atmospheric aerosols remains  
45 feeble at best. This is problematic because aerosols belong to an intricate and tangled  
46 atmospheric system where the aerosol number concentrations range from few thousands to  
47 several hundreds of thousands of particles per cubic centimeter (1/cm) [17,18]. This represents  
48 a Brobdingnagian number of potential surfaces for gas-phase I<sub>2</sub>-particle heterogeneous  
49 reactivity, a hypothesis that has been supported by early laboratory experiments [19–22] that  
50 show that gas phase I<sub>2</sub> readily adsorbs on solid atmospheric particles. Further, we showed in a  
51 recent study that the photodegradation rate of molecular iodine on solid media was very  
52 different (much lower) from the photodegradation rate in the homogeneous phase [23]. This

53 difference in reactivity will likely have a direct impact on the long-range gas-phase I<sub>2</sub>  
54 atmospheric transport and reactive fate [24,25]. That is, different environmental factors may  
55 influence the atmospheric behavior and fate of molecular iodine adsorbed on solid particles.  
56 For example, particles exposed to RH values ranging from 30% to 100% at ambient temperature  
57 may result in surface mono- or multi-layer water films [26]. These surface water layers may  
58 induce important changes in the heterogeneous reactivity since the kinetics of many surface  
59 reactions depend strongly on the type of particle phase, surface morphology and surface  
60 physico-chemical properties [27]. Further, in the case of an accidental radioiodine release from  
61 a nuclear powerplant facility, its dispersion and atmospheric behavior will need to be reassessed  
62 to ensure the radioprotection of the population and application of the appropriate mitigation  
63 strategies.

64 In this work we focus on the kinetics of the photodegradation of molecular iodine adsorbed on  
65 model solid media as function temperature and humidity. Only stable iodine-127 isotope is  
66 studied and the reactivity of the radioisotope iodine-131 is not considered. This allowed us to  
67 carry out all the laboratory experiments without any significant radiological safety concerns.  
68 Further, since iodine-127 and iodine-131 have the same number of valence electrons, their  
69 reactivity is expected to be equivalent. However, the heterogeneous photo-reactivity of the  
70 molecular iodine adsorbed on solid media may be affected by the difference in the molar masses  
71 of iodine-127 and iodine-131. It is not believed that the kinetic isotope effect (KIE) resulting  
72 from the mass-dependence of collision frequencies plays a major role in the heterogeneous  
73 interactions of molecular iodine [28,29]. While the KIE has been shown to play a role in the  
74 homogeneous reactions of OH radicals with non-methane hydrocarbons containing C-12 and  
75 C-13 isotopes [30,31], this effect has been shown to be relatively low (1‰ to ~16‰) for carbon  
76 isotopes [30,32]. Also, the KIE is expected to decrease with increasing molecular mass [30].

77 Consequently, it is assumed that the KIE due to the small difference between the molecular  
78 mass of iodine-127 and iodine-131 is negligible [28,29].

79 The apparatus and the experimental protocol used to study the photo-degradation of molecular  
80 iodine on solid media has been documented before [23]. Therefore, only details relevant to this  
81 work are given below.

## 82 **Experimental**

83 A schematic representation of the experimental system used in this work is published elsewhere  
84 [23]. A 500 cm<sup>3</sup> Pyrex bulb attached to a modified rotary evaporator (Laborota 4000 efficient,  
85 Heidolph) was used to study the heterogeneous photodegradation of molecular iodine adsorbed  
86 on solid SiO<sub>2</sub> particles in the presence of solar radiation in the ultraviolet and visible region of  
87 the solar spectrum [23]. Under typical experimental conditions, about 500 mg of dried SiO<sub>2</sub>  
88 particles coated with molecular iodine was placed within the Pyrex bulb. The bulb was attached  
89 to the modified rotary evaporator and immersed in a temperature-controlled bath. The Xenon  
90 Lamp 300W was used to irradiate the sample within the Pyrex bulb across its wall. The bulb  
91 was allowed to rotate to ensure that the I<sub>2</sub>-coated particles within the Pyrex bulb were well  
92 homogenized, assuring that all the particles were well exposed to the incoming UV and visible  
93 radiation.

94 A continuous flow of synthetic air was allowed to enter the bulb volume. The synthetic air  
95 was generated using a benchtop zero air generator. Briefly, zero air generators produce  
96 laboratory grade purified air by completely removing hydrocarbons, CO<sub>2</sub>, NO<sub>x</sub> (NO<sub>x</sub> = NO +  
97 NO<sub>2</sub>) and H<sub>2</sub>O from the air stream. This avoids the need to use inconvenient air cylinders,  
98 which may be dangerous for laboratory conditions.

99 The total air flow (250 sccm) was controlled using a mass flow controller and the bulb volume  
100 was renewed every two minutes. The experimental flow dynamics were limited by the rate of

101 desorption of molecular iodine adsorbed on the solid media and the gas-particle exchange. That  
102 is, the given gas flow rate was used in order to renew the bulb gaseous volume fast enough (to  
103 avoid a significant I<sub>2</sub> re-adsorption on the silica and to limit a gas-silica equilibrium) without  
104 accelerating the physico-desorption in an unreasonable manner (it would prevent us from  
105 obtaining a reliable estimation of the photodissociation rate or *J*-value (see Equation 1). Part  
106 of the main flow was diverted using a restriction needle valve and allowed to enter two bubblers  
107 placed in a series and filled with ultra-pure water to obtain the desired humidity. The relative  
108 humidity was measured directly in the gas flow using a hygrometer “Hygrolog NT2” (Rotronic)  
109 with “HygroClip SC04” probe. The instrument accuracy of relative humidity measurements  
110 was ±1.5%.

111 Two sets of experiments were carried out. In the first set of experiments, the measured  
112 temperature within the Pyrex bulb was  $T = (298 \pm 1) \text{K}$  and the resulting relative humidity ranged  
113 from  $\leq 2\%$  to 75% RH under given experimental conditions. In the second set of experiments,  
114 the measured relative humidity within the Pyrex bulb was 40% RH and the temperature ranged  
115 from  $283 \pm 1 \leq T(\text{K}) \leq 323 \pm 1$ , values representative of the typical lower atmosphere conditions.

#### 116 SiO<sub>2</sub> particles

117 To simulate the complex physical and chemical nature of atmospheric aerosol content,  
118 AEROSIL R812 silica particles were used [23] to study the influence of the temperature and  
119 relative humidity on the heterogeneous photo-degradation of I<sub>2</sub>. These model particles were  
120 chosen because it has been estimated that as much as 20 to 30% of the atmospheric particles'  
121 content includes SiO<sub>2</sub>. The siloxane surface of the AEROSIL R812 silica particles is, therefore,  
122 a good first approximation of the inorganic oxide particle content found in the atmosphere and  
123 will assist the scientific community to advance the understanding of chemisorption and reactive  
124 fate of molecular iodine adsorbed on aerosols in the atmosphere. The AEROSIL R812

125 (Silanamine, 1,1,1-trimethyl-N-(trimethylsilyl)-, hydrolysis products with silica; CAS Number:  
126 68909-20-6) was purchased from Evonic Degussa GmbH and the stated minimum SiO<sub>2</sub> content  
127 was  $\geq 99.8\%$ . AEROSIL R812 is a fumed silica aftertreated with organosilane with high  
128 specific surface and marked hydrophobia. The stated specific surface area (based on Brunauer-  
129 Emmett-Teller (BET) analysis conducted at the boiling temperature of N<sub>2</sub>, 77K) was  $260 \pm 30$   
130 m<sup>2</sup>/g (AEROSIL, 2014, p. 812) and the stated average particle size was 7 nm. However, the  
131 SiO<sub>2</sub> particles are known to agglomerate to form an aerosol of a few micrometers in diameter,  
132 reflecting atmospheric-like suspended matter [33]. Particle density was 60 g/L.

### 133 Coating of SiO<sub>2</sub> particles

134 Molecular iodine was coated on the SiO<sub>2</sub> particles surface using a liquid/solid adsorption  
135 method as reported in our earlier work [23]. The particles coating was carried out in the absence  
136 of UV visible radiation to minimize any photo-degradation of molecular iodine. In a typical  
137 coating procedure, 500 mg of SiO<sub>2</sub> particles were placed within the 500 cm<sup>3</sup> Pyrex bulb and  
138 100 mL of 9 mg/L I<sub>2</sub>/cyclohexane (HPLC grade,  $\geq 99.8\%$ , Sigma-Aldrich) solution was added  
139 to the mix. The bulb with its contents was then placed in an ultrasonic bath for 15 minutes to  
140 homogenize the mixture. After, the liquid cyclohexane fraction of the mix was removed under  
141 aspirator vacuum (Rotavapor R-114, Büchi) at  $T = 313\text{K}$  and  $p = (25.6 \pm 2)$  MPa for 45 minutes.  
142 Assuming a uniform particle surface coverage for the iodine molecules and a spherical particle  
143 geometry, the percentage of the particle surface coated with iodine was estimated to be  $\sim 0.2\%$   
144 of the monolayer for hydrophobic silica [34].

### 145 Extraction and molecular iodine quantification

146 Similar to our previous work [23], the 2,4,6-tribromoaniline internal standard and the N,N-  
147 dimethylaniline derivatization reagent were used to quantify the molecular iodine adsorbed on  
148 solid SiO<sub>2</sub> particles. Under typical experimental conditions, 30 mg of the sample was extracted

149 from the Pyrex bulb every 30 minutes and placed in an air-tight vial. After, 50  $\mu$ L of the internal  
150 standard and 50  $\mu$ L of the 300 mg/L N,N-dimethylaniline/cyclohexane solution was added to  
151 the vial. The vial was then hermetically sealed and stored at  $T = -20^{\circ}\text{C}$  until the following day.  
152 Subsequently, contents of the vial were placed in a stainless-steel compartment volume of the  
153 Accelerated Solvent Extraction (ASE 300, Dionex) system and topped-off with 33 mL of  
154 cyclohexane solvent. Three ASE cycles were performed. The first 5-minute cycle of the ASE  
155 extraction process was allowed to take place at  $T = 100^{\circ}\text{C}$  and  $p = 100$  bar. After, 50% (~16.5  
156 mL) of the ASE cell volume was automatically extracted and then resulting aliquot was placed  
157 in a separate ASE stainless-steel compartment volume. The original ASE cell was then topped-  
158 off with cyclohexane to 33 mL total volume. The extraction process was then repeated two  
159 more times. After the final, third, cycle, the total volume of the ASE cell was retrieved (33 mL).  
160 The net final volume (~70 mL) was then enriched under a steady flow of nitrogen gas using the  
161 TurboVapII (Biotage) workstation. The nitrogen gas flow temperature was kept at  $T = 50^{\circ}\text{C}$   
162 and the  $\text{N}_2$ -gas head pressure was  $p = 5$  bar. The obtained extract solution was concentrated  
163 down to a final volume of 500  $\mu$ L. The obtained 500  $\mu$ L extract was then filtered using a PTFE  
164 (0.22  $\mu\text{m}$  pore size) membrane filter and analyzed using the TRACE GC Ultra gas  
165 chromatography (Thermo Scientific) and quantified using the TSQ Quantum Triple Quadrupole  
166 Mass Spectrometer (Thermo Scientific). A Thermo TG-5MS capillary column (30 m  $\times$  0.25  
167 mm i.d., 0.25  $\mu\text{m}$ ) was used. The helium (99.999%, Air Liquide) carrier gas flow rate was 1  
168 mL/min. Liquid samples were injected in the split mode (1:50) and the injector temperature was  
169 maintained at  $T = 220^{\circ}\text{C}$ . The initial GC oven temperature was held at  $T = 35^{\circ}\text{C}$  for one minute  
170 and then the oven temperature was stepped-up at the rate of 30  $^{\circ}\text{C}/\text{min}$  to 220 $^{\circ}\text{C}$  and then held  
171 at  $T = 220^{\circ}\text{C}$  for 11 minutes. The transfer line temperature between the GC and the MS/MS  
172 analyzer was  $T = 280^{\circ}\text{C}$ . The MS/MS analyzer was operated in a full scan/single ion monitoring

173 mode to increase the sensitivity and the MS/MS system electron impact ionization energy was  
174 70 eV.

### 175 Photolytic light source

176 Similar to our previous work [23], the 300 W high pressure Xenon lamp (LOT, Oriel) was used  
177 as the solar radiation source to irradiate the I<sub>2</sub>-SiO<sub>2</sub> mixture located within the Pyrex reactor.  
178 The Xenon lamp solar radiation spectrum and the discussion concerning the radiometric  
179 measurements within the Pyrex reactor are published elsewhere [23].

## 180 **Results and discussion**

### 181 Rate of photolysis of I<sub>2</sub>

182 Similar to our previous work [23], the kinetics of the heterogeneous photolysis of I<sub>2</sub> on SiO<sub>2</sub>  
183 particles were determined by monitoring the loss of I<sub>2</sub> as a function of time. The photolytic loss  
184 of molecular iodine adsorbed on SiO<sub>2</sub> particles exhibited an exponential decay, implying first-  
185 order kinetics (Equation 1).

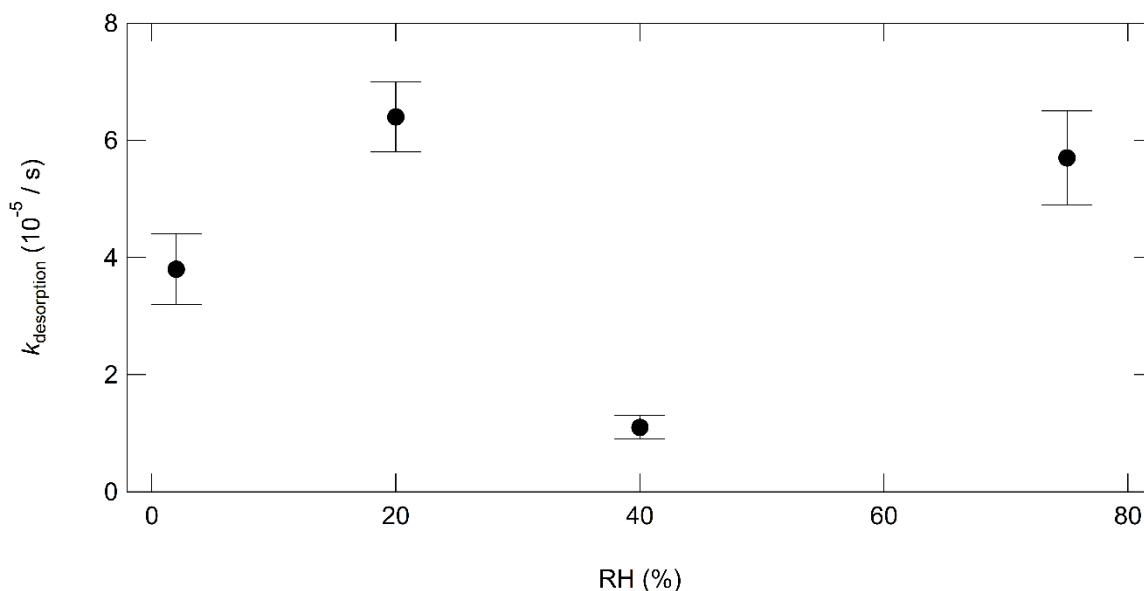
$$186 \quad \frac{d[I_2]}{dt} = -k_{\text{obs}} [I_2] = -(k_{\text{desorption}} + J)[I_2] \quad (1)$$

187 In Equation. 1,  $k_{\text{obs}}(\text{s}^{-1})$  is the observed first-order rate constant,  $k_{\text{desorption}}(\text{s}^{-1})$  is the desorption  
188 first-order rate constant,  $J(\text{s}^{-1})$  is the photodissociation rate constant,  $t(\text{s})$  is the time of exposure  
189 to solar radiation and  $[I_2]$  is the normalized iodine concentration adsorbed on the silica particles.

### 190 “Dark” desorption and hydrolysis of iodine adsorbed on SiO<sub>2</sub> particles

191 Since the vapor pressure of solid molecular iodine is about  $33.3 \leq p(\text{Pa}) \leq 41.3$  [35–37] at  $T =$   
192  $20^\circ\text{C}$ , part of the initial amount of I<sub>2</sub> adsorbed on SiO<sub>2</sub> particles will certainly volatilize over  
193 time. To account for this loss of iodine due to desorption and/or hydrolysis ( $k_{\text{desorption}}$ ),  
194 background control experiments were carried out in the absence of photolytic radiation under

195 given experimental conditions of temperature and relative humidity. As shown in an earlier  
196 study, heterogeneous reactivity of pendimethalin adsorbed on AEROSIL R812 particles was  
197 observed to decrease with increasing relative humidity [38]. To account for this “hydrophobic”  
198 effect, experiments were carried out at  $T = 298\text{K}$  and relative humidity (RH) values ranging  
199 from  $\leq 2\%$  to  $75\%\text{RH}$ . Values of first-order kinetic constants  $k_{\text{desorption}}$  at different humidity  
200 values are presented in the Table 1 and shown in Figure 1. As presented in Table 1 and  
201 illustrated in Figure 1, the first-order rate constant  $k_{\text{desorption}}$  accounts for the background  
202 desorption of  $\text{I}_2$  from the  $\text{SiO}_2$  surface, hydrolysis of  $\text{I}_2$  due to a presence of water on  $\text{SiO}_2$   
203 surfaces and other losses. As shown in Figure 1, no clear dependence of  $k_{\text{desorption}}$  on relative  
204 humidity is observed. Two reproducibility experiment were performed at  $0\%$  and  $20\%\text{RH}$  and  
205 led to a desorption kinetics values well within the uncertainty bars shown in Figure 1. As a  
206 result, iodine loss observed in our experimental conditions are expected to be due to desorption  
207 rather than hydrolysis; hydrolysis is expected to occur for higher RH values than those studied  
208 in this work.



209  
210 *Figure 1 Plot of the obtained first-order rate constants ( $k_{\text{desorption}}$ ) for the desorption of iodine*  
211 *as a function of relative humidity. No clear dependence of humidity on the desorption rate*  
212 *constant of  $\text{I}_2$  adsorbed on  $\text{SiO}_2$  particles is observed. The quoted uncertainties in  $k_{\text{desorption}}$ ,*  
213 *values are  $68\%$  ( $1\sigma$ ) confidence limits from the linear regression fit.*

214 Influence of humidity on the photo-degradation of I<sub>2</sub> on SiO<sub>2</sub> particles ( $k_{\text{obs}}$ )

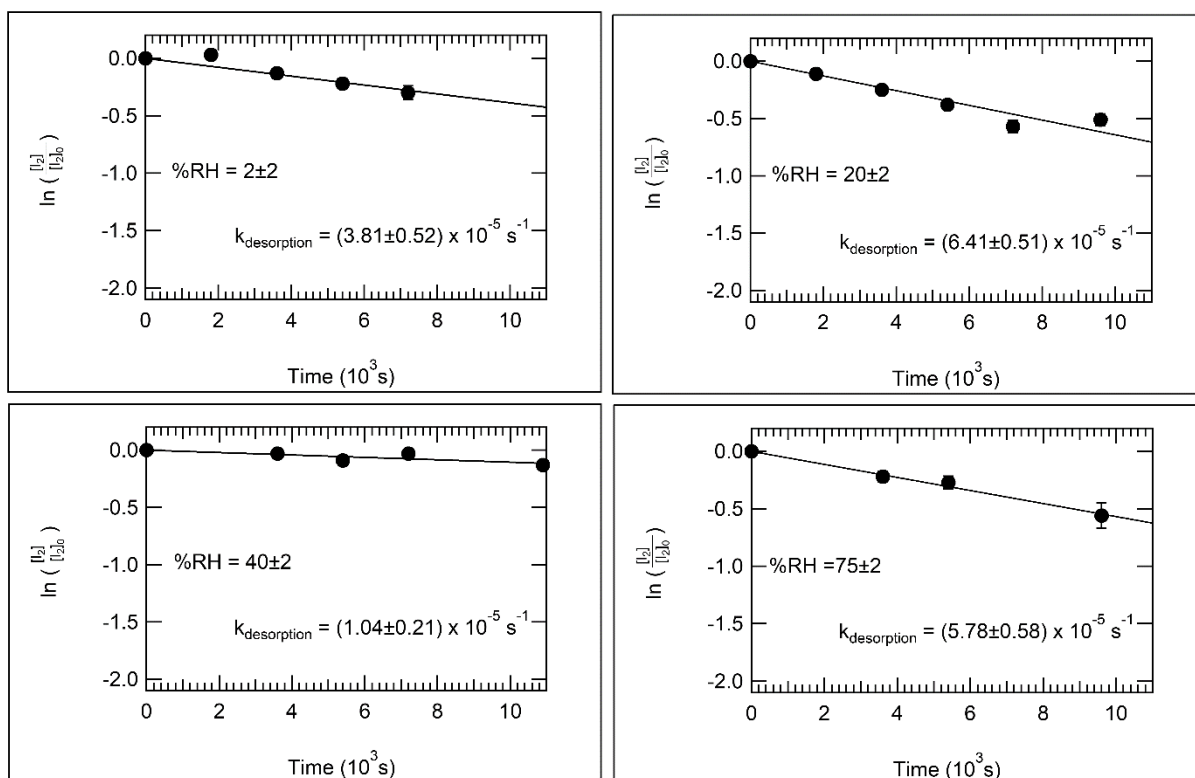
215 It is known that water in all its phases plays an important role in global warming and  
 216 atmospheric chemistry. Water is a known green-house gas, albeit all-important and  
 217 indispensable for life on Earth, and an atmospheric precursor of hydroxyl radicals responsible  
 218 for the oxidative capacity of the atmosphere. Further, it is known that mono- and multi-layer  
 219 water films form on atmospheric particles when the relative humidity is 30% or greater [26].  
 220 This is important since the kinetics of many heterogeneous, surface or interface reactions  
 221 depend on the type of aerosol particle phase and surface morphology and physico-chemical  
 222 properties and behavior [27]. As a result, the influence of humidity on the photo-oxidation of  
 223 I<sub>2</sub> on SiO<sub>2</sub> particles ( $k_{\text{obs}}$ ) is studied.

224 Typical normalized iodine concentration temporal profiles for experiments carried out at  $T =$   
 225 298K and  $\leq 2$  to 75%RH in the absence (“dark” conditions) and presence of simulated solar  
 226 radiation are shown in shown in Figure 2 and Figure 3, respectively. The obtained  $k_{\text{desorption}}$  and  
 227  $k_{\text{obs}}$  rate constants are listed in Table 1.

228 *Table 1. Summary of kinetic data for the photolysis of I<sub>2</sub> adsorbed on SiO<sub>2</sub> particles carried out*  
 229 *at  $T = 298\text{K}$  and (2 - 75)%RH in a Pyrex reactor and using 300W Xe lamp photolysis. The*  
 230 *listed errors in %RH are estimated systematic errors associated with measuring the relative*  
 231 *humidity. The quoted uncertainties in the  $k_{\text{desorption}}$ ,  $k_{\text{observed}}$  and  $J$  values are 68% ( $1\sigma$ )*  
 232 *confidence limits from the linear regression fit. <sup>1</sup>: Dark condition. <sup>2</sup>: Xe lamp photolysis*

%RH	$k_{\text{desorption}}^1$ (10 <sup>-5</sup> /s)	$k_{\text{observed}}^2$ (10 <sup>-5</sup> /s)	$J$ (10 <sup>-5</sup> /s)	$\tau$ (min)
2±2	3.8±0.6	11.1±1.1	7.3±1.2	228
20±2	6.4±0.6	13.4±1.6	7.0±1.0	238
40±2 <sup>§</sup>	1.1±0.2	10.0±1.1	8.9±1.1	187
75±2	5.7±0.8	14.9±1.6	9.2±1.1	160

233 <sup>§</sup> [23]

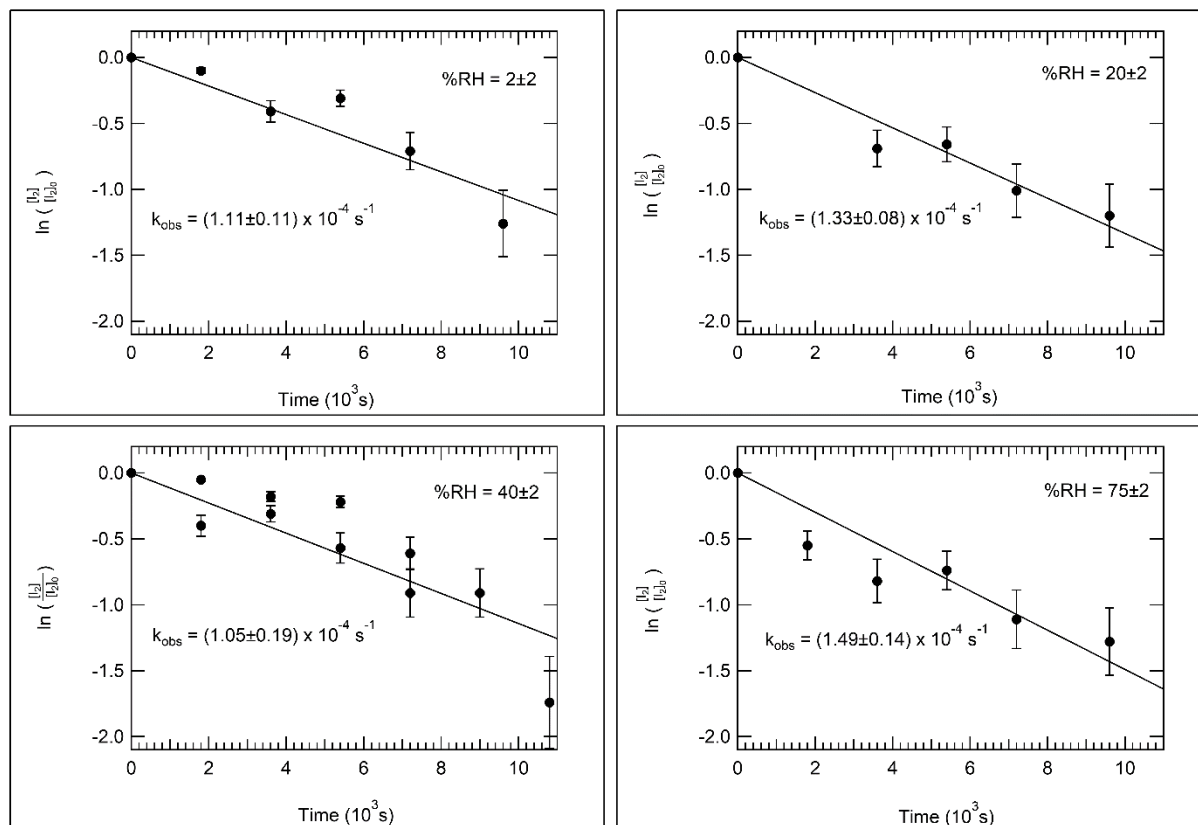


234

235 *Figure 2. Typical normalized iodine concentration temporal profiles for experiments carried*  
 236 *out at  $T = 298\text{K}$  and  $\leq 2$  to  $75$  %RH in the absence of simulated solar radiation (“dark”*  
 237 *conditions). The solid lines are obtained from least squares analyses and give the expressions*  
 238 *for  $k_{\text{desorption}}$  shown in the figure. The error bars in %RH are estimated systematic errors*

239 associated with measuring the relative humidity. The quoted uncertainties in  $k_{obs}$  are 68% ( $1\sigma$ )  
 240 confidence limits from the linear regression fit.

241



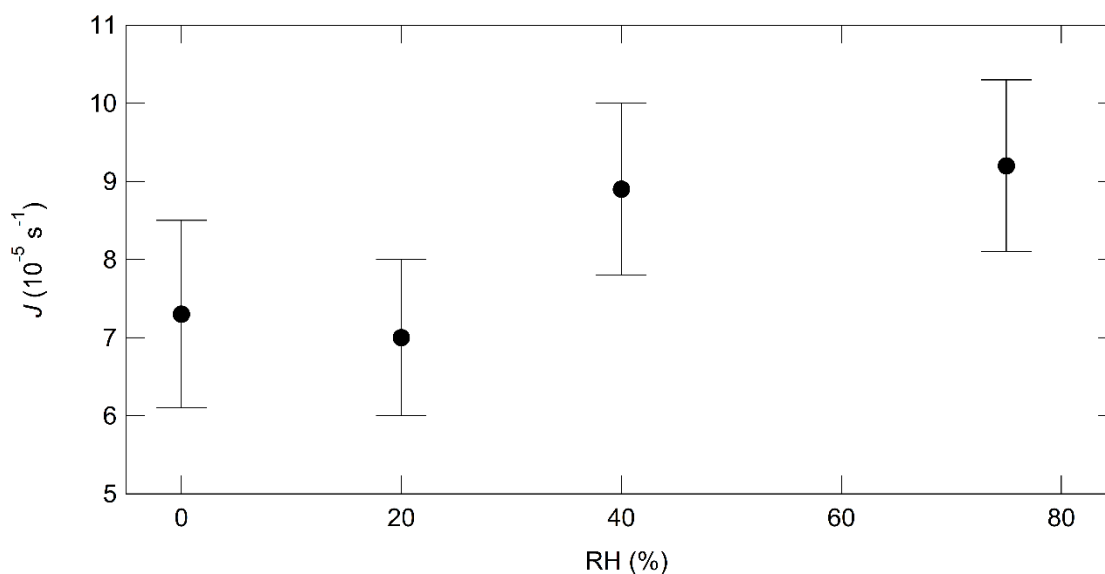
242

243 *Figure 3. Typical normalized iodine concentration temporal profiles for experiments carried*  
 244 *out at  $T = 298K$  and (2 - 75)%RH following photolysis of the  $I_2$  adsorbed on  $SiO_2$  particles.*  
 245 *The solid lines are obtained from least squares analyses and give the expressions for  $k_{obs}$  shown*  
 246 *in the figure. The error bars in %RH are estimated systematic errors associated with measuring*  
 247 *the relative humidity. The quoted uncertainties in  $k_{obs}$  are 68% ( $1\sigma$ ) confidence limits from the*  
 248 *linear regression fit.*

249 As listed in Table 1, the photodissociation rate constant,  $J$ , for  $I_2$  adsorbed on  $SiO_2$  particles, is  
 250 obtained from the difference in the desorption rate constant,  $k_{desorption}$ , and the observed  
 251 photolysis rate constant,  $k_{obs}$  (see Equation 1). The  $k_{desorption}$  accounts for 10% to 50% of the  
 252 observed  $k_{obs}$  which is small enough to quantify in a relevant manner the photodissociation rate  
 253 constant,  $J$ -value, and confirms that the given experimental gas flow rate within the bulb is  
 254 appropriate for these experiments. Plot of the obtained first-order rate constants for the  
 255 heterogeneous photolysis of iodine as a function of relative humidity is shown in Figure 4. As

256 shown in Figure 4, no clear dependence of the photodissociation rate constant on relative  
257 humidity is observed. As a result, the average photodissociation rate constant is calculated to  
258 give  $J = (8.2 \pm 1.1) \times 10^{-5}/s$  at  $T=298K$  independent of relative humidity under the  
259 experimental conditions employed. Based on the obtained  $J$ -value, the photolytic lifetime of  $I_2$   
260 adsorbed on  $SiO_2$  particles is calculated to be approximately 203 minutes or 3.4 hours.

261 The absence of the dependence on humidity of the photodissociation rate constant of  $I_2$  adsorbed  
262 on  $SiO_2$  particles may be explained by its low solubility (300 mg/L) in water [36,39]. Further,  
263 the observed non-dependence may also be explained by the type of  $SiO_2$  particles used in this  
264 work, that is, hydrophobic AEROSIL R812 silica particles. These particles are known to  
265 prevent water film formation on their surfaces. However, these “hydrophobic” effect on  
266 AEROSIL R812 silica particles may decrease with increasing gas-phase water content. Further,  
267 these types of “hydrophobic” particles are often used by atmospheric scientists to study real-  
268 life atmospheric behavior of aerosols. At higher humidity levels, the water surface coverage of  
269 AEROSIL R812 silica particles is known to approach real-life atmospheric particle physiology.  
270 Nonetheless, to confirm the obtained results in this work, other types of particles with different  
271 surface physico-chemical characteristics that better represent the complex nature of  
272 atmospheric aerosols need to be studied.



273

274 *Figure 4. Plot of the obtained first-order rate constants for the heterogeneous photolysis of*  
 275 *iodine as a function of relative humidity. No clear influence of humidity on the*  
 276 *photodissociation rate constant of  $I_2$  adsorbed on  $SiO_2$  particles is observed.*

277

#### 278 Influence of the temperature on the photo-degradation of $I_2$ on $SiO_2$ particles

279 To better understand the real atmosphere behavior and fate of molecular iodine adsorbed on  
 280 solid particles, a set of heterogeneous photolysis experiments was performed at different  
 281 temperatures that reflect more realistic environment conditions [40]. Typical normalized iodine  
 282 concentration temporal profiles for experiments carried out at 40%RH and  $283 \leq T(K) \leq 323$   
 283 temperature range under “dark” conditions and following the photolysis of the  $I_2/SiO_2$  solid are  
 284 shown in Figure 5 and Figure 6, respectively. As shown in Figure 5, the  $k(T)_{\text{desorption}}$  values are  
 285 obtained from experiments carried out under “dark” conditions, that is, in the absence of solar  
 286 radiation. In a similar manner, as shown in Figure 6, the  $k(T)_{\text{obs}}$  values are obtained from  
 287 experiments in the presence of simulated solar radiation. The obtained  $k(T)_{\text{desorption}}$  and  $k(T)_{\text{obs}}$   
 288 rate constants are listed in Table 2.

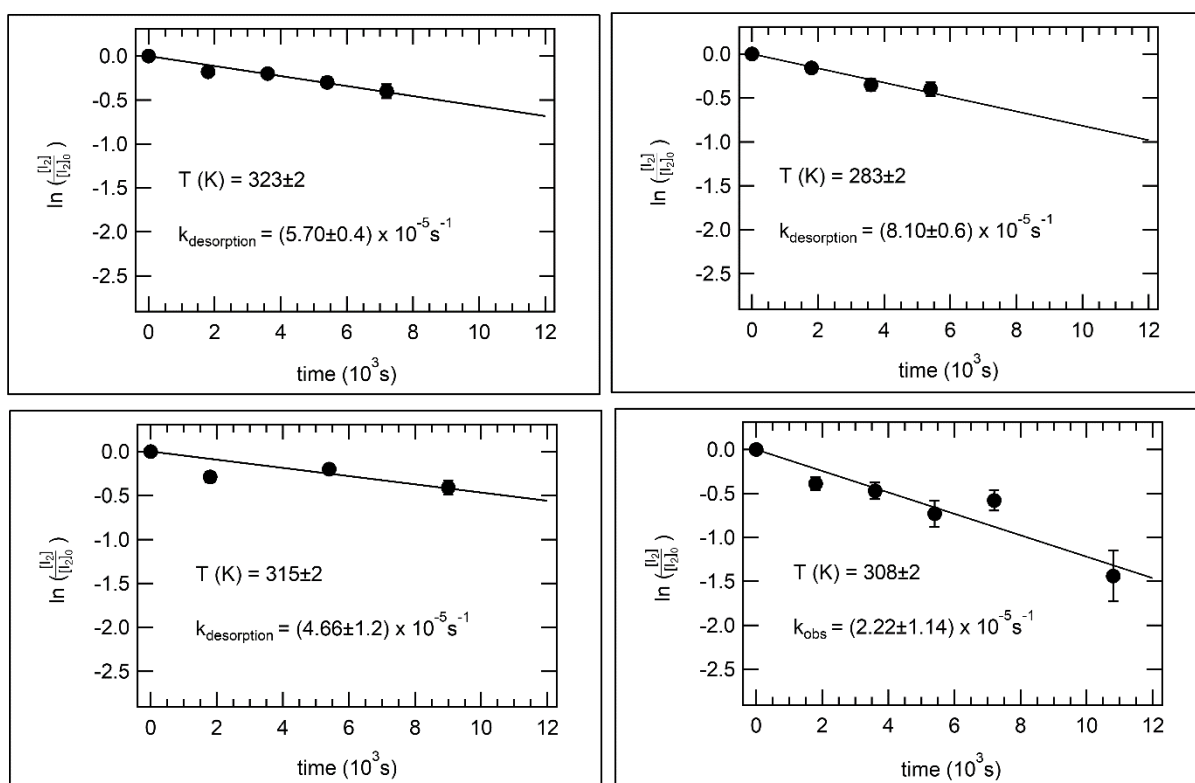
289 *Table 2 Summary of kinetic data for the photolysis of  $I_2$  adsorbed on  $SiO_2$  particles carried out*  
 290 *at the  $283 \leq T(K) \leq 323$  temperature range and at 40%RH in a Pyrex reactor and using 300W*  
 291 *Xe lamp photolysis. The listed errors in temperature are estimated systematic errors associated*

292 with the measurement. The quoted uncertainties in the  $k_{\text{desorption}}$ ,  $k_{\text{observed}}$  and  $J$  values are 68%  
 293 ( $1\sigma$ ) confidence limits from the linear regression fit. <sup>1</sup>: Dark condition. <sup>2</sup>: Xe lamp photolysis

T (K)	$k_{\text{desorption}}^1$ ( $10^{-5}/\text{s}$ )	$k_{\text{observed}}^2$ ( $10^{-5}/\text{s}$ )	$J$ ( $10^{-5}/\text{s}$ )	$\tau^{\&}$ (min)
283±2	8.1±0.6	14.7±1.1	6.6±1.3	252
298±2 <sup>§</sup>	1.1±0.1	10±1.1	8.9±1.1	187
308±2	12.1±1.1	22.2±1.4	10.1±1.1	165
315±2	4.6±1.2	14.1±1.1	9.5±1.6	175
323±2	5.7±0.8	19.8±1.8	14.1±1.8	119

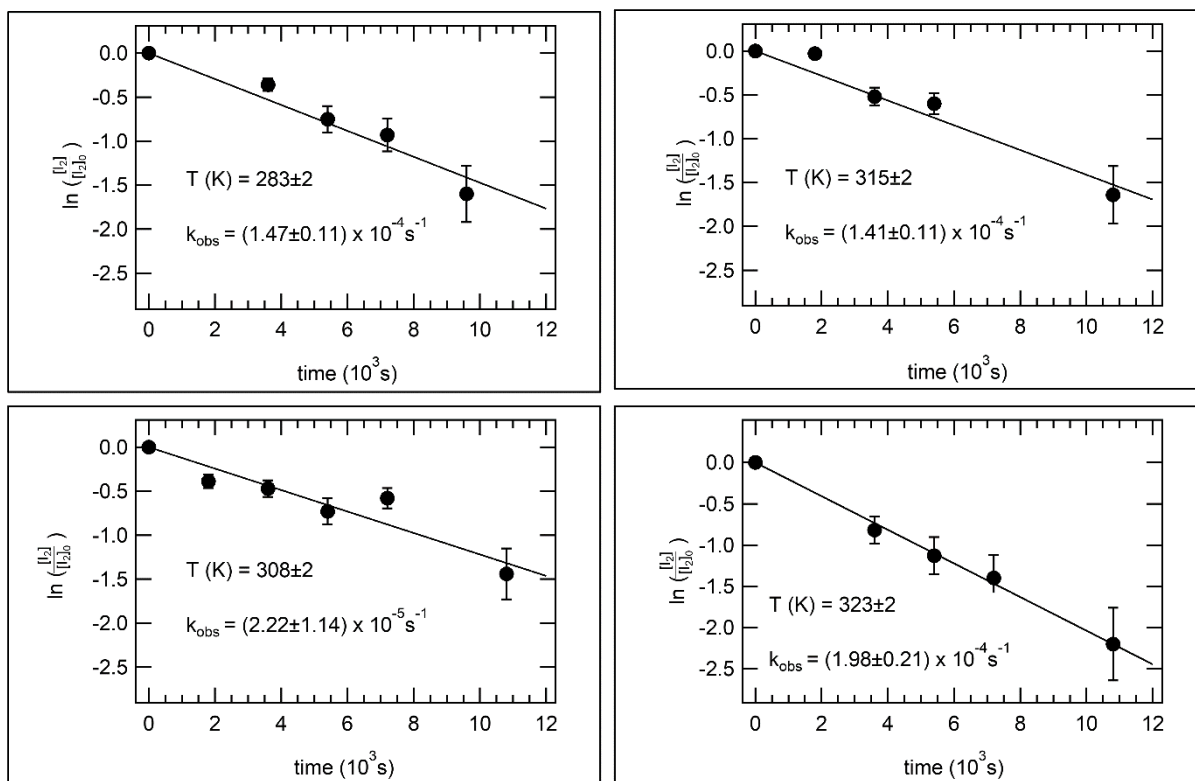
294 <sup>§</sup> [23]

295 <sup>&</sup> The atmospheric residence time  $\tau = 1/J(T)$



296

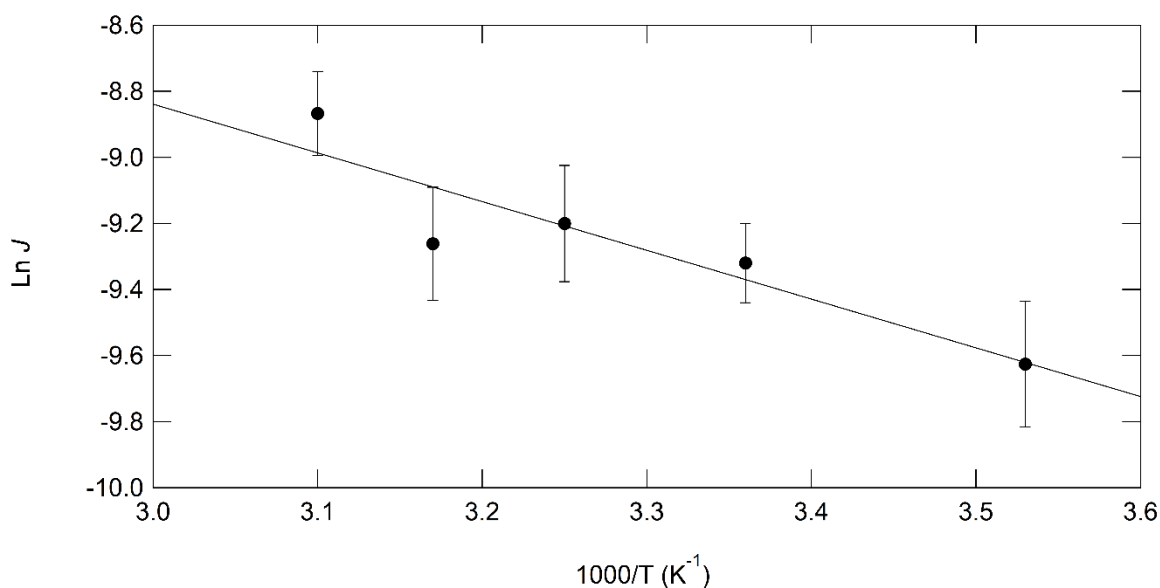
297 Figure 5. Typical normalized iodine concentration temporal profiles for experiments carried  
 298 out in the  $283 \leq T(K) \leq 323$  temperature range and at 40%RH in the absence of photolysis  
 299 ("dark" conditions) of the  $I_2$  adsorbed on  $SiO_2$  particles.



300

301 *Figure 6 Typical normalized iodine concentration temporal profiles for experiments carried*  
 302 *out in the  $283 \leq T(K) \leq 323$  temperature range and at 40%RH following photolysis of the  $I_2$*   
 303 *adsorbed on  $SiO_2$  particles. The solid lines are obtained from least squares analyses and give*  
 304 *the expressions for  $k_{obs}$  shown in the figure. The quoted uncertainties in the  $k_{observed}$  values are*  
 305 *68% ( $1\sigma$ ) confidence limits from the linear regression fit.*

306 Similar to the situation listed above, the photodissociation rate constant,  $J(T)$ , for  $I_2$  adsorbed  
 307 on  $SiO_2$  particles, is calculated from the difference in the experimentally obtained desorption  
 308 rate constant,  $k_{desorption}$ , and the experimentally obtained rate constant,  $k_{obs}$ . The  
 309 photodissociation rate constant ( $J$ -value) for the photo-degradation of  $I_2$  on solid  $SiO_2$  particles  
 310 does not appear to be humidity dependent under the experimental conditions employed ( $< 55\%$   
 311 of the total contribution). On the other hand, the  $J$ -value for the photo-degradation of  $I_2$  on solid  
 312  $SiO_2$  particles is observed to be temperature dependent in the temperature range  $T = 283K$  to  $T$   
 313  $= 323K$ . Plot of the obtained natural logarithm of the obtained  $J(K)$  value for the heterogeneous  
 314 photolysis of molecular iodine as a function of temperature is shown in Figure 7. As shown in  
 315 Figure 7, a clear dependence of the photodissociation rate constant on temperature is observed.



316

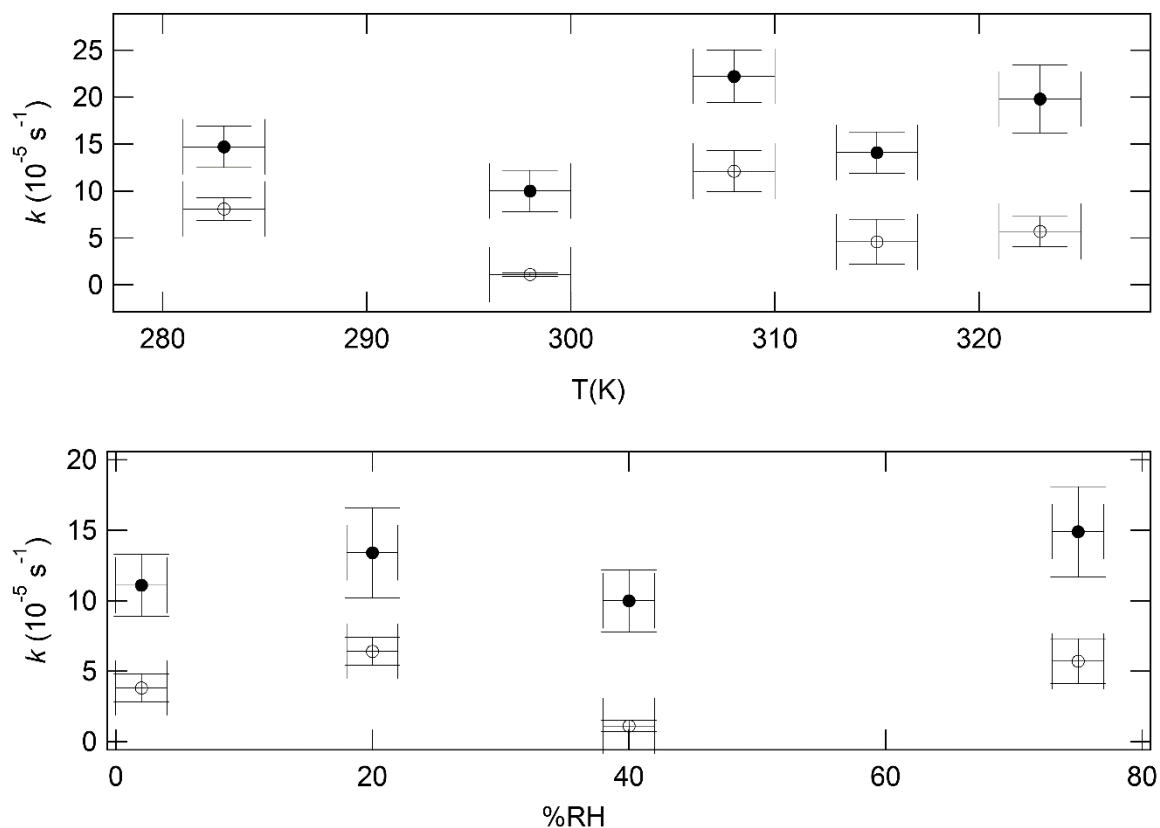
317 *Figure 7 Arrhenius plot for photolysis of the I<sub>2</sub> adsorbed on SiO<sub>2</sub> particles. The solid line is*  
 318 *obtained from a least-squares analysis and given the following Arrhenius expression:*  
 319  *$J(T) = (1.24 \pm 1.4) \times 10^{-2} \times \exp[(1482 \pm 345)/T] /s$ . The uncertainties in the expression*  
 320 *are 1σ and represent precision only.*

321 The following Arrhenius expression is derived from the data:

322 
$$J(T) = (1.24 \pm 1.4) \times 10^{-2} \times \exp[(1482 \pm 345)/T] \text{ s}^{-1}$$

323 Uncertainties in the above expression are ±1σ and represent precision only and refer to the  
 324 Arrhenius parameters only. The activation energy for the photodissociation reaction of I<sub>2</sub> on  
 325 SiO<sub>2</sub> particles is rounded-off to be 12.3±2.9 kJ/mol.

326 As stated above, the  $J(T)$  value is calculated from the difference in the experimentally obtained  
 327 desorption rate constant,  $k_{\text{desorption}}$ , and the experimentally obtained rate constant,  $k_{\text{obs}}$ . As listed  
 328 in Table 1 and Table 2 and shown in the Figure 8 below, there is no clear humidity dependence  
 329 on the obtained  $k_{\text{desorption}}$  and  $k_{\text{obs}}$  values. However, such an influence on humidity of the  
 330 obtained  $k$ -values cannot be excluded.



332

333 *Figure 8. Comparison of the experimentally obtained desorption rate constant,  $k_{\text{desorption}}$ , (○*  
 334 *open circles) and the experimentally obtained rate constant,  $k_{\text{obs}}$  values (● closed circles) as a*  
 335 *function of temperature (above) and relative humidity (below). The uncertainties in the  $k$  values*  
 336 *are 95% ( $2\sigma$ ) confidence limits. The uncertainties in the temperature are  $\pm 2\text{K}$ , experimental*  
 337 *estimation.*

338 On the other hand, as shown in Figure 8, while there does not appear to be a clear temperature  
 339 dependence on the  $k_{\text{desorption}}$  values, the obtained  $k_{\text{obs}}$  rate constants do appear to be temperature  
 340 dependent. The observed discrepancies may be explained by the physico-chemical surface  
 341 properties of the AEROSIL R812 particles used in this work. That is, the AEROSIL R812  
 342 surfaces are coated with organo-silane compounds and treated at  $T=105^\circ\text{C}$  for 2 hours before  
 343 being commercialized. The AEROSIL surfaces are thus assumed to be chemically inert and  
 344 “stable” under the experimental conditions (283K-323K) employed in this work. Nevertheless,  
 345 chemical rearrangements on the AEROSIL R812 surfaces cannot be fully excluded that may  
 346 have induced the observed influence of the  $k_{\text{desorption}}$  (dark conditions) on the experimental the

347 %RH and temperature. As a result, the physico-chemical interactions of I<sub>2</sub> on silica surfaces  
348 may differ at given experimental RH and temperature conditions. However, the observed  
349 influence of the temperature seems to have only a minor effect on the estimation of the  
350 photolysis rate constant as shown in Figure 7.

### 351 **Conclusion**

352 The heterogeneous photodegradation of I<sub>2</sub> on solid surfaces was studied at  $T(K) = 283$  to  $T(K)$   
353  $= 323K$  and from  $\leq 2\%RH$  to  $\leq 75\%RH$  in synthetic air to better understand its atmospheric  
354 fate. The results reported in this work demonstrate that the calculated  $J$ -value is observed to be  
355 temperature dependent over the temperature range studied. This photolysis rate constant may  
356 be expressed by  $J(T) = (1.24 \pm 1.4) \times 10^{-2} \times \exp[(1482 \pm 345)/T] /s$  over the measured  
357 temperature range. The heterogeneous atmospheric residence time ( $\tau=1/J(T)$ ) of I<sub>2</sub> adsorbed on  
358 solid media is calculated to range from 2 to 4.1 hours.

359 This work complements and completes the previous study on the photodegradation of molecular  
360 iodine adsorbed on model SiO<sub>2</sub> particles [23]. The obtained results will help to improve the  
361 calculation of the evolution of molecular iodine dispersion and transport in the atmosphere.  
362 More generally, the obtained results will help the industrial and academic communities to better  
363 understand and predict the environmental fate of I<sub>2</sub> adsorbed on the particle surfaces. However,  
364 to better understand and model real-atmosphere heterogeneous behavior of I<sub>2</sub>, other studies  
365 need to be included that include other particle surfaces with different physico-chemical  
366 properties to better understand and model the atmospheric dispersion and environmental fate of  
367 I<sub>2</sub>.

### 368 **Acknowledgements**

369 We gratefully acknowledge financial support in a form of a doctoral grant from the *Institut de*  
370 *Radioprotection et de Sûreté Nucléaire* (IRSN) and the *Region Sud*.

371 **Nomenclature**

372	CCN	=	cloud condensation nuclei
373	eV	=	electron volt
374	HPLC	=	High Performance Liquid Chromatography
375	$J(T)$	=	photolysis rate constant (1/s) as a function of temperature, $T$ .
376	KIE	=	Kinetic Isotope Effect
377	$k_{\text{desorption}}$	=	desorption first-order-rate constant (1/s)
378	$k_{\text{obs}}$	=	observed first-order-rate constant (1/s)
379	mg	=	milligram
380	$\mu\text{L}$	=	microliter
381	mL	=	milliliter
382	MS	=	mass spectrometry
383	MS/MS	=	tandem mass spectrometry
384	%RH	=	percent relative humidity
385	pptv	=	parts per trillion per volume
386	$\sigma$	=	standard deviation
387	$t$	=	time (s)
388	W	=	Watt

389

390 **References**  
391

- 392 [1] Buseck, P. R., and Pósfai, M., 1999, “Airborne Minerals and Related Aerosol Particles:  
393 Effects on Climate and the Environment,” *Proc. Natl. Acad. Sci.*, 96(7), pp. 3372–3379.
- 394 [2] Baker, A. R., Thompson, D., Campos, M. L. A. M., Parry, S. J., and Jickells, T. D., 2000,  
395 “Iodine Concentration and Availability in Atmospheric Aerosol,” *Atmos. Environ.*,  
396 34(25), pp. 4331–4336.
- 397 [3] Garland, J. A., and Curtis, H., 1981, “Emission of Iodine from the Sea Surface in the  
398 Presence of Ozone,” *J. Geophys. Res. Oceans*, 86(C4), pp. 3183–3186.
- 399 [4] Saiz-Lopez, A., Plane, J. M. C., Baker, A. R., Carpenter, L. J., Von Glasow, R., G Omez  
400 Martín, J. C., Mcfiggans, G., and Saunders, R. W., 2012, “Atmospheric Chemistry of  
401 Iodine,” *Chem Rev*, 112, pp. 1773–1804.
- 402 [5] Bitter, M., Ball, S. M., Povey, I. M., and Jones, R. L., 2005, “A Broadband Cavity  
403 Ringdown Spectrometer for In-Situ Measurements of Atmospheric Trace Gases,”  
404 *Atmospheric Chem. Phys.*, 5(9), pp. 2547–2560.
- 405 [6] Finley, B. D., and Saltzman, E. S., 2008, “Observations of Cl<sub>2</sub>, Br<sub>2</sub>, and I<sub>2</sub> in Coastal  
406 Marine Air,” *J. Geophys. Res. Atmospheres*, 113(D21).
- 407 [7] Huang, R.-J., Seitz, K., Buxmann, J., Pöhler, D., Hornsby, K. E., Carpenter, L. J., Platt,  
408 U., and Hoffmann, T., 2010, “In Situ Measurements of Molecular Iodine in the Marine  
409 Boundary Layer: The Link to Macroalgae and the Implications for O<sub>3</sub>, IO, OIO and NO  
410 x,” *Atmospheric Chem. Phys.*, 10(10), pp. 4823–4833.
- 411 [8] Leigh, R. J., Ball, S. M., Whitehead, J., Leblanc, C., Shillings, A. J. L., Mahajan, A. S.,  
412 Oetjen, H., Lee, J. D., Jones, C. E., and Dorsey, J. R., 2010, “Measurements and Modelling  
413 of Molecular Iodine Emissions, Transport and Photodestruction in the Coastal Region  
414 around Roscoff,” *Atmospheric Chem. Phys.*, 10(23), pp. 11823–11838.
- 415 [9] Mahajan, A. S., Oetjen, H., Saiz-Lopez, A., Lee, J. D., McFiggans, G. B., and Plane, J.  
416 M., 2009, “Reactive Iodine Species in a Semi-polluted Environment,” *Geophys. Res. Lett.*,  
417 36(16).
- 418 [10] Mahajan, A. S., Plane, J. M. C., Oetjen, H., Mendes, L., Saunders, R. W., Saiz-Lopez, A.,  
419 Jones, C. E., Carpenter, L. J., and McFiggans, G. B., 2010, “Measurement and Modelling  
420 of Tropospheric Reactive Halogen Species over the Tropical Atlantic Ocean,”  
421 *Atmospheric Chem. Phys.*, 10(10), pp. 4611–4624.
- 422 [11] Peters, C., Pechtl, S., Stutz, J., Hebestreit, K., Hönninger, G., Heumann, K., Schwarz, A.,  
423 Winterlik, J., and Platt, U., 2005, “Reactive and Organic Halogen Species in Three  
424 Different European Coastal Environments,” *Atmospheric Chem. Phys.*, 5(12), pp. 3357–  
425 3375.
- 426 [12] Saiz-Lopez, A., Saunders, R. W., Joseph, D. M., Ashworth, S. H., and Plane, J. M. C.,  
427 2004, *Atmospheric Chem. Phys. Discussions*, 4, pp. 2379-2403.
- 428 [13] Saiz-Lopez, A. J. M. C. P., Plane, J. M. C., McFiggans, G., Williams, P. I., Ball, S. M.,  
429 Bitter, M., Jones, R. L., Hongwei, C., and Hoffmann, T., 2006, “Modelling Molecular  
430 Iodine Emissions in a Coastal Marine Environment: The Link to New Particle Formation,”  
431 *Atmospheric Chem. Phys.*, 6(4), pp. 883–895.
- 432 [14] Kinoshita, N., Sueki, K., Sasa, K., Kitagawa, J., Ikarashi, S., Nishimura, T., Wong, Y.-S.,  
433 Satou, Y., Handa, K., Takahashi, T., and others, 2011, “Assessment of Individual  
434 Radionuclide Distributions from the Fukushima Nuclear Accident Covering Central-East  
435 Japan,” *Proc. Natl. Acad. Sci.*, 108(49), pp. 19526–19529.
- 436 [15] Momoshima, N., Sugihara, S., Ichikawa, R., and Yokoyama, H., 2012, “Atmospheric  
437 Radionuclides Transported to Fukuoka, Japan Remote from the Fukushima Dai-Ichi

- 438 Nuclear Power Complex Following the Nuclear Accident,” *J. Environ. Radioact.*, 111, pp.  
439 28–32.
- 440 [16] Loewenstein, L. M., and Anderson, J. G., 1985, “Rate and Product Measurements for the  
441 Reactions of Hydroxyl with Molecular Iodine and Iodine Chloride at 298 K: Separation  
442 of Gas-Phase and Surface Reaction Components,” *J. Phys. Chem.*, 89(25), pp. 5371–5379.
- 443 [17] Koutsenogii, P. K., and Jaenicke, R., 1994, “Number Concentration and Size Distribution  
444 of Atmospheric Aerosol in Siberia,” *J. Aerosol Sci.*, 25(2), pp. 377–383.
- 445 [18] Sharma, D., Rai, J., Israil, M., and Singh, P., 2003, “Summer Variations of the  
446 Atmospheric Aerosol Number Concentration over Roorkee, India,” *J. Atmospheric Sol.-  
447 Terr. Phys.*, 65(9), pp. 1007–1019.
- 448 [19] Chamberlain, A. C., 1960, “Aspects of the Deposition of Radioactive and Other Gases and  
449 Particles,” *Intern J Air Pollut.*, 3.
- 450 [20] Chamberlain, A. C., and Chadwick, R. C., 1966, “Transport of Iodine from Atmosphere  
451 to Ground,” *Tellus*, 18(2–3), pp. 226–237.
- 452 [21] Gard, E. E., 1998, “Direct Observation of Heterogeneous Chemistry in the Atmosphere,”  
453 *Science*, 279(5354), pp. 1184–1187.
- 454 [22] Shen, X., Zhao, Y., Chen, Z., and Huang, D., 2013, “Heterogeneous Reactions of Volatile  
455 Organic Compounds in the Atmosphere,” *Atmos. Environ.*, 68, pp. 297–314.
- 456 [23] Figueiredo, A., Streckowski, R. S., Bosland, L., Durand, A., and Wortham, H., 2020,  
457 “Photolytic Degradation of Molecular Iodine Adsorbed on Model SiO<sub>2</sub> Particles,” *Sci.  
458 Total Environ.*, p. 137951.
- 459 [24] Garland, J. A., 1967, “The Adsorption of Iodine by Atmospheric Particles,” *J. Nucl.  
460 Energy*, 21(9), pp. 687–700.
- 461 [25] Megaw, W. J., 1965, “The Adsorption of Iodine on Atmospheric Particles,” *J. Nucl.  
462 Energy. Parts A/B. React. Sci. Technol.*, 19(8), pp. 585–592.
- 463 [26] Keskinen, H., Romakkaniemi, S., Jaatinen, A., Miettinen, P., Saukko, E., Jorma, J.,  
464 Mäkelä, J. M., Virtanen, A., Smith, J. N., and Laaksonen, A., 2011, “On-Line  
465 Characterization of Morphology and Water Adsorption on Fumed Silica Nanoparticles,”  
466 *Aerosol Sci. Technol.*, 45(12), pp. 1441–1447.
- 467 [27] Knipping, E. M., 2000, “Experiments and Simulations of Ion-Enhanced Interfacial  
468 Chemistry on Aqueous NaCl Aerosols,” *Science*, 288(5464), pp. 301–306.
- 469 [28] Coenen, H. H., Mertens, J., and Mazieère, B., 2006, *Radiation Reactions For  
470 Pharmaceuticals. Compendium for Effective Synthesis Strategies*, Springer Netherlands.
- 471 [29] Deitz, V. R., 1987, “Interaction of Radioactive Iodine Gaseous Species with Nuclear-  
472 Grade Activated Carbons,” *Carbon*, 25(1), pp. 31–38.
- 473 [30] Rudolph, J., Czuba, E., and Huang, L., 2000, “The Stable Carbon Isotope Fractionation  
474 for Reactions of Selected Hydrocarbons with OH-Radicals and Its Relevance for  
475 Atmospheric Chemistry,” *J. Geophys. Res. Atmospheres*, 105(D24), pp. 29329–29346.
- 476 [31] Rudolph, J., Czuba, E., Norman, A. L., Huang, L., and Ernst, D., 2002, “Stable Carbon  
477 Isotope Composition of Nonmethane Hydrocarbons in Emissions from Transportation  
478 Related Sources and Atmospheric Observations in an Urban Atmosphere,” *Atmos.  
479 Environ.*, 36(7), pp. 1173–1181.
- 480 [32] Cantrell, C. A., Shetter, R. E., McDaniel, A. H., Calvert, J. G., Davidson, J. A., Lowe, D.  
481 C., Tyler, S. C., Cicerone, R. J., and Greenberg, J. P., 1990, “Carbon Kinetic Isotope Effect  
482 in the Oxidation of Methane by the Hydroxyl Radical,” *J. Geophys. Res. Atmospheres*,  
483 95(D13), pp. 22455–22462.
- 484 [33] Mattei, C., 2019, “Réactivité hétérogène de pesticides adsorbés sur des particules  
485 atmosphériques : Influence des paramètres environnementaux sur les cinétiques,” *Ph.D.  
486 Thesis*, Aix-Marseille Université.

- 487 [34] Socorro, J., Gligorovski, S., Wortham, H., and Quivet, E., 2015, "Heterogeneous  
488 Reactions of Ozone with Commonly Used Pesticides Adsorbed on Silica Particles,"  
489 *Atmos. Environ.*, 100, pp. 66–73.
- 490 [35] Baxter, G. P., Hickey, C. H., and Holmes, W. C., 1907, "The Vapor Pressure of Iodine,"  
491 *J. Am. Chem. Soc.*, 29(2), pp. 127–136.
- 492 [36] Linstrom, P. J., and Mallard, W. G., 2020, "NIST Chemistry WebBook, NIST Standard  
493 Reference Database Number 69". Available at: <https://doi.org/10.18434/T4D303>.
- 494 [37] Stull, D. R., 1947, "Vapor Pressure of Pure Substances. Organic and Inorganic  
495 Compounds," *Ind. Eng. Chem.*, 39(4), pp. 517–540.
- 496 [38] Mattei, C., Wortham, H., and Quivet, E., 2019, "Heterogeneous Degradation of Pesticides  
497 by OH Radicals in the Atmosphere: Influence of Humidity and Particle Type on the  
498 Kinetics," *Sci. Total Environ.*, 664, pp. 1084–1094.
- 499 [39] Hartley, H., and Campbell, N. P., 1908, "LXIX.—The Solubility of Iodine in Water," *J*  
500 *Chem Soc Trans*, 93(0), pp. 741–745.
- 501 [40] Sander, S. P., 1986, "Kinetics and Mechanism of the Iodine Monoxide + Iodine Monoxide  
502 Reaction," *J. Phys. Chem.*, 90(10), pp. 2194–2199.
- 503